Investigation of Fracturing Process of Rock-Like Brazilian Disks Containing Three Parallel Cracks under Compressive Line Loading

H. Haeri,[a,1] K. Shahriar,[b] M. F. Marji,[c] and P. Moarefvand[b]

[a] Department of Mining Engineering, Science and Research Branch, Islamic Azad University, Tehran, Iran

[b] Department of Mining and Metallurgical Engineering, Amirkabir University of Technology, Tehran, Iran

[c] Faculty of Mining and Metallurgy, Institution of Engineering, Yazd University, Yazd, Iran

[1] hadihaeri@ymail.com

Исследование процесса разрушения образцов типа "бразильского диска" из скальной породы с тремя параллельными трещинами при одноосном сжатии

Х. Хаэри[a,1], К. Шахриар[б], М. Ф. Маржи[в], П. Моарефванд[б]

[a] Факультет горного дела, Отделение научных исследований, Исламский университет Азад, Тегеран, Иран

[б] Факультет горного дела и металлургии, Технологический университет им. Амира Кабира, Тегеран, Иран

[в] Факультет горного дела и металлургии, Отделение машиностроения, Университет г. Йезд, Иран

Выполнены испытания на одноосное сжатие образцов типа "бразильского диска" из скальной породы с тремя предварительно выращенными параллельными трещинами в средней части. Образцы из модельного материала (бетон на основе пуццоланового портландцемента, мелкого песка и воды) изготовляли в лаборатории механики горных пород. Измерения критической нагрузки в таких дисках показали, что она незначительно зависит от ориентации трещин и их взаимовлияния. Процесс разрушения образцов изучали при разных углах наклона трех параллельных трещин относительно оси сжимающей нагрузки по обычной схеме испытаний бразильских дисков. Экспериментально установлено, что на первом этапе нагрузки начинается бифуркация трещин и их распространение в направлении линии сжимающей нагрузки. Проведено численное моделирование процесса разрушения образцов с помощью косвенного метода граничных элементов высшего порядка, известного как "метод разрыва перемещений". Данные численных расчетов по инициированию и слиянию трещин сравнивали с экспериментальными результатами. Получена тесная корреляция численных результатов с экспериментальными.

Ключевые слова: исходные трещины, дисковые образцы, материалы из скальных пород, слияние трещин, экспериментальные работы, численное моделирование.

Introduction. The presence of pre-existing cracks may reduce the fracture toughness of brittle materials [1]. The mechanical behavior of brittle materials may be affected by the micromechanical behavior of cracks. Nevertheless, the extension of cracks depends on the properties of cracks such as size, location, orientation, and loading condition. The initiation

and propagation of cracks play a vital role in predicting the cyclic fracture process of rock specimens [2].

In the crack propagation process of brittle materials, such as precracked rock specimens, usually two types of cracks are observed originating from tips of pre-existing cracks (i.e., wing cracks and secondary cracks). Wing cracks are usually produced due to tension, while secondary cracks may initiate due to shear. Therefore, initiation of wing cracks in rocks is favored relative to secondary cracks because of the lower toughness of these materials in tension than in shear [3]. The pre-existing cracks in rocks are normally under compressive loading rather than under tension, shear or mixed mode loading [4]. It is mainly expected that the crack initiation will follow in the direction (approximately) parallel to the maximum compressive load [5].

Many experimental works have been devoted to study of the crack initiation, propagation path, and eventual coalescence of the pre-existing cracks in specimens made of various substances, including natural rocks or rock-like materials under compressive loading [6–24]. Brazilian disk test is one of the most suitable tests in evaluating the static and dynamic fracture toughness of rocks and rock-like specimens containing central pre-existing crack or cracks. These tests may also be used to study the crack initiation, propagation path and cracks coalescence of brittle substances such as rocks under compressive line loadings [25–33]. This testing procedures used extensively to measure the tensile strength, fracture toughness and mixed mode breakage process in the uncracked and precracked disk specimens of various brittle substances under compressive line loading [34–43]. It should be noted that in Brazilian disk specimens, the crack initiation and fracture process in specimens often happen very soon under compressive line loading due to the low tensile strength of rocks and rock-like materials. For example, Al-Shayea [43] experimentally studied the crack propagation paths in the central straight through crack in Brazilian disk (CSCBD) specimens of brittle limestone with different crack inclination angles under mixed mode I/II loading and investigated the influence of confining pressure and temperature on the crack initiation and propagation of the rock specimens. The experimental results were compared with theoretical predictions of crack initiation angles. Ghazvinian et al. [33] have performed analytical, experimental, and numerical studies for a better understanding of crack propagation process in the CSCBD specimens under compressive line loading. The existing experimental and numerical analyses also confirmed the effect of crack inclination angle and crack length on fracturing processes of brittle materials under various loading conditions.

Various numerical methods have been developed for simulation of crack propagation in brittle substances, e.g., finite element method (FEM), boundary element method (BEM), discrete element method (DEM), etc. Three important fracture initiation criteria were proposed to study the crack propagation mechanism of brittle materials, i.e., (I) the maximum tangential stress (σ_θ-criterion) [44], (ii) the maximum energy release rate (*G*-criterion) [45], and (iii) the minimum energy density criterion (*S*-criterion) [46]. Some modified form of the above criteria, e.g., *F*-criterion which is a modified form of energy release rate criterion proposed by Shen and Stephansson [47] may also be used to study the breakage behavior of brittle substances [48–50]. Several computer codes were used to model the breakage mechanism of brittle materials such as rocks, for example, FROCK code [17], Rock Failure Process Analysis (RFPA[2D]) code [51], 2D Particle Flow Code (PFC[2D]) [23, 33, 52].

However, in most of the published investigations usually specimens with a single center crack have been studied. In the present study, the Brazilian disks of rock-like materials containing three parallel cracks in the central part of the specimen are analyzed both experimentally and numerically. The precracked disk specimens [prepared from portland pozzolana cement (PPC), fine sands, and water] are tested under compressive line loading. The stress and displacement fields, the crack propagation and crack coalescence

through the specimens and in the bridge area (the area between the three cracks in the specimens containing three cracks) of precracked rock-like disk specimens have been studied both experimentally and numerically. Some of the experimental works are simulated numerically by a modified higher-order displacement discontinuity method, while crack propagation and crack coalescence in the bridge area are studied based on Mode I and Mode II stress intensity factors (SIFs). The experimental data are compared with the numerical results, which are in good agreement with each other and illustrate the accuracy and validity of the present work.

1. **Specimen Preparation and Testing**. Initiation, propagation and coalescence of the pre-existing cracks in rock-like specimens have been experimentally investigated by many researchers [15–17]. One of the most difficult tasks in experimental investigations is the preparation of specimens containing cracks. The rock-like disk specimens are specially prepared from a mixture of PCC, fine sands, and water. The diameter and thickness of the precracked rock-like disk specimens prepared for experimental tests are 100 and 30 mm, respectively (Fig. 1).

Table 1 gives the mechanical properties of the prepared rock-like specimens tested in the rock mechanics laboratory before inserting the cracks.

T a b l e 1
Some Mechanical Properties of the Uncracked Rock-Like Disk Specimens

Characteristic	Parameter	Value
Compressive strength	σ_c, MPa	28
Tensile strength	σ_t, MPa	3.81
Young modulus	E, GPa	15
Poisson's ratio	ν	0.21

Fig. 1. A typical rock-like disk specimen.

Note that the tensile strength (σ_t) for uncracked rock-like disk specimens is

$$\sigma_t = \frac{2F}{\pi BR},$$

where F is the applied compressive load in kN, B is thickness of the disk specimen, and R is radius of the disk specimen.

Various Brazilian disk tests were conducted on rock-like disk specimens containing three parallel cracks. These cracks are created by inserting three thin metal shims with 10 mm width and 1 mm thickness into the specimens during their casting in a mold.

The disk specimens with three cracks are prepared in such a manner that the cracks are parallel to each other and oriented at different angles to the load line, i.e., at the angles $\varphi = 0, 15, 30, 45, 70,$ and $90°$ (in a counterclockwise direction) as schematically shown in
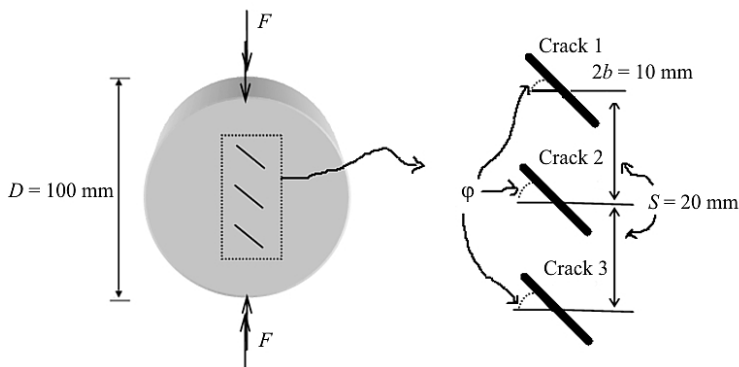
Fig. 2 Geometry of three parallel cracks in a rock-like disk specimen under compression.

Fig. 2. The compressive line loading F was diametrically applied, and the loading rate of 0.5 MPa/s was maintained during the tests.

Figure 2 demonstrates a schematic view of the geometry of three parallel cracks (i.e., *crack 1*, *crack 2*, and *crack 3*, respectively) with equal lengths $2b = 10$ mm and the crack length-to-diameter ratio $b/D = 0.1$.

In this study, six specimens were prepared. Three parallel cracks are located at the centerline of each specimen with the spacing of 20 mm ($S = 20$ mm). Spacing is taken as the vertical distance between the centers of two cracks expressed in mm.

2. **Experimental Procedures and Results**. The specially prepared (rock-like) specimens are tested experimentally, and the results are used to analyze the breaking loads and the crack propagation process of the precracked disk specimens.

2.1. *Breaking Stress Analysis of the Precracked Disk Specimens*. It is obvious that the precracked rock-like disk specimens have a lower strength as compared to uncracked specimens.
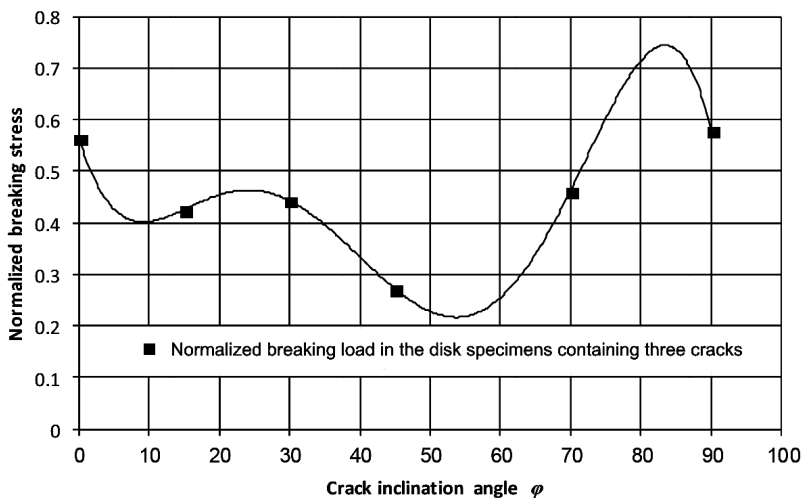

Fig. 3. Normalized breaking stress versus $\varphi = 0, 15, 30, 45, 70,$ and $90°$.

The breaking stress analysis of the precracked disk specimens containing three parallel cracks with different orientations is of paramount importance to study the behavior of brittle materials. The stresses causing new crack initiation and the crack coalescence were also observed. Figure 3 describes the normalized breaking stress variation for six

cases: $\varphi = 0$, 15, 30, 45, 70, and 90°. The final breaking stress of the precracked disk specimens is normalized by the average breaking stress of the uncracked specimens. The average breaking stress of uncracked specimens is about 3.81 MPa. The normalized breaking stress for the six cases $\varphi = 0$, 15, 30, 45, 70, and 90° is usually less than one because the pre-existing crack may reduce the final strength of specimen (Fig. 3). As shown in Fig. 3, normalized breaking stress in $\varphi = 0$ to 70° and $\varphi = 90°$ is larger than that at different stages of crack propagation process with other inclination angles.

Thus, fracture toughness mode is more critical than tensile breakage mode in the precracked disk specimens. It should be noted that in $\varphi = 30°$, pure shear mode loading was obtained and then the value of breakage load increased.

2.2. ***Crack Propagation of Precracked Disk Specimens***. Crack coalescence phenomenon may occur when the three pre-existing cracks combine due to propagation of wings and/or secondary cracks (originating from the tips of pre-existing cracks) in brittle substances under various compressive loadings. As shown in Fig. 4, crack coalescence in the bridge area may also occur during the crack propagation process.

$\varphi = 0$
a

$\varphi = 15°$
b

$\varphi = 30°$
c

$\varphi = 45°$
d

$\varphi = 70°$
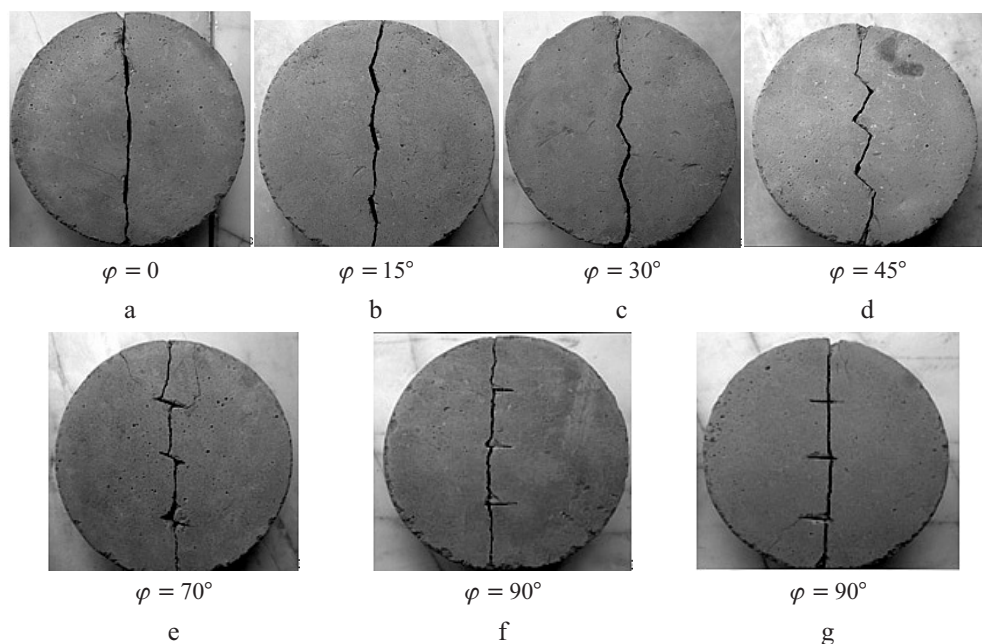e

$\varphi = 90°$
f

$\varphi = 90°$
g

Fig. 4. Experimental results illustrating the coalescence path of rock-like disk specimens containing three pre-existing cracks.

In the current experimental study, wing cracks are instantaneously initiated quasi-statically (Fig. 4). The development and coalescence of wing cracks in the bridge area (i.e., the area in-between the three pre-existing cracks) may be the main cause of fracture paths in rock-like disk specimens.

The bridge areas may be considered as the areas starting from the tips of pre-existing cracks for the cases shown in Fig. 4a–d ($\varphi = 0$, 15, 30, and 45°). It should be noted that for the case shown in Fig. 4e–g ($\varphi = 70$ and 90°) the cracks may not be initiated at the tips of pre-existing cracks. For $\varphi = 90°$, the specimen might fail due to two possible crack propagation processes starting from the right/left tips of pre-existing cracks in a tensile splitting mode.

Figure 4a–g shows the observed wing cracks propagating toward each other and causing crack coalescence in the bridge areas.

Figure 4a–g illustrates six cases of coalescence paths due to the propagation of the wing cracks in the bridge areas that are experimentally observed.

3. **Numerical Simulation of the Precracked Specimens by Indirect Boundary Element Method**.

3.1. *Numerical Method*. A displacement-based version of the indirect boundary element method known as displacement discontinuity method (DDM), which was originally proposed by Crouch [53] for the solution of elastostatic problems in solid mechanics, is used in this study [54–58].

A higher accuracy of the displacement discontinuities along the boundary is obtained by using quadratic displacement discontinuity (DD) elements. A quadratic DD element is subdivided into three equal subelements, such that each subelement contains a central node for which the nodal DD is evaluated numerically [48, 49].
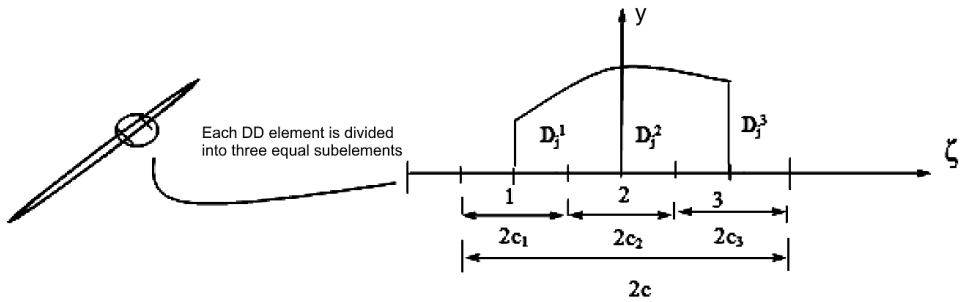

Fig. 5. Quadratic collocations for the higher order displacement discontinuity variation.

Figure 5 shows the displacement distribution at the quadratic collocation point 'm', which can be calculated as

$$D_j(\zeta) = \Sigma A_m(\zeta) D_j^m, \qquad j = x, \ y, \qquad m = 1, \ 2, \ 3, \tag{1}$$

where D_j^1, D_j^2, and D_j^3 are the quadratic nodal displacement discontinuities in x and y directions. Considering a quadratic element of length, $2c$, with equal subelements ($c_1 = c_2 = c_3$) and a quadratic shape function, $A_m(\zeta)$ for $-c \leq \zeta \leq c$, the following shape functions of the quadratic collocation point 'm' can be defined [48],

$$A_1(\varepsilon) = \zeta(\zeta - 2c_1)/8c_1^2, \quad A_2(\zeta) = -(\zeta^2 - 4c_1^2)/4c_1^2, \quad A_3(\zeta) = \zeta(\zeta + 2c_1)/8c_1^2. \tag{2}$$

The stresses and displacements for a straight crack in an infinite specimen along the x-axis, in terms of single harmonic functions $f(x, y)$ and $g(x, y)$, are given by crouch and star field [45] as

$$\sigma_{xx} = 2\rho[2f,_{xy} + y f,_{xyy}] + 2\rho[g,_{yy} + y g,_{yyy}],$$
$$\sigma_{yy} = 2\rho[-y f,_{xyy}] + 2\rho[g,_{yy} - y g,_{yyy}], \tag{3}$$
$$\sigma_{xy} = 2\rho[2f,_{yy} + y f,_{yyy}] + 2\rho[-y g,_{xyy}],$$

and the displacements are

$$u_x = [2(1-\nu)f,_y - y f,_{xx}] + [-(1-2\nu)g,_x - y g,_{xy}],$$
$$u_y = [(1-2\nu)f,_x - y f,_{xy}] + [2(1-\nu)g,_y - y g,_{yy}], \tag{4}$$

where ρ is shear modulus and $f_{,x}$, $g_{,x}$, $f_{,y}$, $g_{,y}$, etc. are the partial derivatives of the single harmonic functions $f(x,\,y)$ and $g(x,\,y)$ with respect to x and y. These potential functions (for the quadratic variation of DD along the element) can be written as

$$f(x,\,y) = \frac{-1}{4\pi(1-\nu)} \sum_{m=1}^{3} D_x^m \Omega_m (I_0,\, I_1,\, I_2),$$

$$g(x,\,y) = \frac{-1}{4\pi(1-\nu)} \sum_{m=1}^{3} D_y^m \Omega_m (I_0,\, I_1,\, I_2). \tag{5}$$

The common function Ω_m, can be defined as

$$\Omega_m (I_0,\, I_1,\, I_2) = \int A_m(\zeta) \ln\,[(x-\zeta)+y^2]^{1/2}\, d\zeta, \qquad m = 1 \text{ to } 3. \tag{6}$$

The integrals I_0, I_1, and I_2 in Eq. (6) can be obtained as

$$I_0(x,\,y) = \int_{-c}^{c} \ln\,[(x-\zeta)^2 + y^2]^{1/2}\, d\zeta =$$

$$= y(\psi_1 - \psi_2) - (x-c)\ln(\Gamma_1) + (x+c)\ln(\Gamma_2) - 2c, \tag{7a}$$

$$I_1(x,\,y) = \int_{-c}^{c} \zeta \ln\,[(x-\zeta)^2\, y^2]^{1/2}\, d\zeta =$$

$$= xy(\psi_1 - \psi_2) + 0.5\,(y^2 - x^2 + c^2)\ln(\Gamma_1/\Gamma_2) - cx, \tag{7b}$$

$$I_2(x,\,y) = \int_{-c}^{c} \zeta^2 \ln\,[(x-\zeta)^2 + y^2]^{1/2}\, d\zeta = \frac{y}{3}(3x^2 - y^2)(\psi_1 - \psi_2) +$$

$$+ \frac{1}{3}(3xy^2 - x^3 + c^3)\ln(\Gamma_1) - \frac{1}{3}(3xy^2 - x^3 - c^3)\ln(\Gamma_2) - \frac{2c}{3}\left(x^2 - y^2 + \frac{c^2}{3}\right), \tag{7c}$$

where ψ_1, ψ_2, Γ_1, and Γ_2 can be derived as

$$\psi_1 = \arctan\left(\frac{y}{x-c}\right), \qquad \psi_2 = \arctan\left(\frac{y}{x+c}\right), \qquad \Gamma_1 = [(x-c)^2 + y^2]^{1/2},$$

$$\Gamma_2 = [(x+c)^2 + y^2]^{1/2}. \tag{8}$$

In order to eliminate the singularity of the displacements, provide stress calculation near the crack ends, and increase the accuracy of order-higher displacement discontinuity method around the original crack tip, a special treatment of the crack at the tip is necessary [48, 49]. In previous works, usually, one or two elements for the specific crack tip was/were used, but in the present study three special crack tip elements at the crack ends are used in the general higher-order displacement discontinuity method. As shown in Fig. 6, the DD variation for three nodes can be formulated using a special crack tip element containing three nodes (or having three special crack tip subelements) [48],
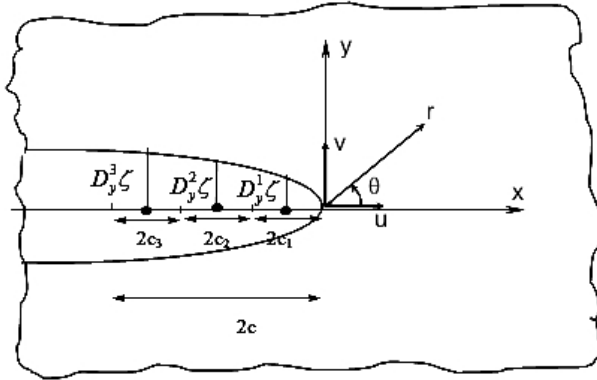
Fig. 6. A special crack tip element with three equal subelements.

$$D_j(\zeta) = \sum A_{Tm}(\zeta) D_j^m(c), \qquad j = x, \ y, \qquad m = 1, \ 2, \ 3. \tag{9}$$

Considering a crack tip element with the three equal subelements ($c_1 = c_2 = c_3$), the shape functions $A_{T1}(\zeta)$, $A_{T2}(\zeta)$, and $A_{T3}(\zeta)$ can be obtained as equations:

$$A_{T1}(\zeta) = \frac{15\zeta^{1/2}}{8c_1^{1/2}} - \frac{\zeta^{3/2}}{c_1^{3/2}} + \frac{\zeta^{5/2}}{8c_1^{5/2}}, \qquad A_{T2}(\zeta) = \frac{-5\zeta^{1/2}}{4\sqrt{3}c_1^{1/2}} + \frac{3\zeta^{3/2}}{2\sqrt{3}c_1^{3/2}} - \frac{\zeta^{5/2}}{4\sqrt{3}c_1^{5/2}},$$

$$A_{T3}(\zeta) = \frac{3\zeta^{1/2}}{8\sqrt{5}c_1^{1/2}} - \frac{\zeta^{3/2}}{2\sqrt{5}c_1^{3/2}} + \frac{\zeta^{5/2}}{8\sqrt{5}c_1^{5/2}}. \tag{10}$$

The common function $\Omega_T^m(I_T^1, I_T^2, I_T^3)$ is defined as

$$\Omega_T^m(I_T^m) = \int_{-c}^{c} A_{Tm}(\zeta) \ln[(x - \zeta)^2 + y^2]^{1/2} d\zeta, \qquad m = 1, \ 2, \ 3. \tag{11}$$

The integrals I_T^1, I_T^2, and I_T^3 can be expressed as

$$I_T^1(x, \ y) = \int_{-c}^{c} \zeta^{1/2} \ln[(x - \zeta)^2 + y^2]^{1/2} d\zeta,$$

$$I_T^2(x, \ y) = \int_{-c}^{c} \zeta^{3/2} \ln[(x - \zeta)^2 + y^2]^{1/2} d\zeta, \tag{12}$$

$$I_T^3(x, y) = \int_{-c}^{c} \zeta^{5/2} \ln[(x - \zeta)^2 + y^2]^{1/2} d\zeta.$$

The Mode I and Mode II stress intensity factors K_I and K_{II} can be estimated based on the linear elastic fracture mechanics (LEFM) theory as the opening and sliding displacements [48]:

$$K_I = \frac{\rho}{4(1 - \nu)} \left(\frac{2\pi}{c}\right)^{1/2} D_y(c), \qquad K_{II} = \frac{\rho}{4(1 - \nu)} \left(\frac{2\pi}{c}\right)^{1/2} D_x(c). \tag{13}$$

3.2. ***Numerical Simulation of the Experimental Works***. A modified higher-order displacement discontinuity method based on the versatile boundary element method [48] is used for the numerical simulation of the proposed experimental works (i.e., to study the crack coalescence in the bridge area and crack propagation process of brittle substances under compressive line loading). Six different specimens (Fig. 4a–g) are numerically simulated by the proposed numerical method, and the results are plotted in Fig. 7a–g. The LEFM approach based on the concept of SIFs proposed by Irwin [59] is implemented in the boundary element code and the maximum tangential stress criterion given by Erdogan and Sih [44] are used in a stepwise procedure to estimate the propagation path of wing cracks. An iterative method explained by Marji [60] has been used to investigate the crack propagation directions and paths after each crack extension step, $\Delta b = 0.1b$, successively. The propagation path of each crack has been estimated by this iterative method, and finally the coalescence of the cracks has been observed (after propagation of wing cracks). As it follows from the results shown in Fig. 7, the numerically simulated propagation paths are in good agreement with the corresponding experimentally observed paths (Fig. 4). It should be noted that the numerical results are based on the crack propagation process originating from the cracks tips but as shown in Fig. 4, while some experimental specimens do not include any wing cracks starting from the tips of horizontal cracks.
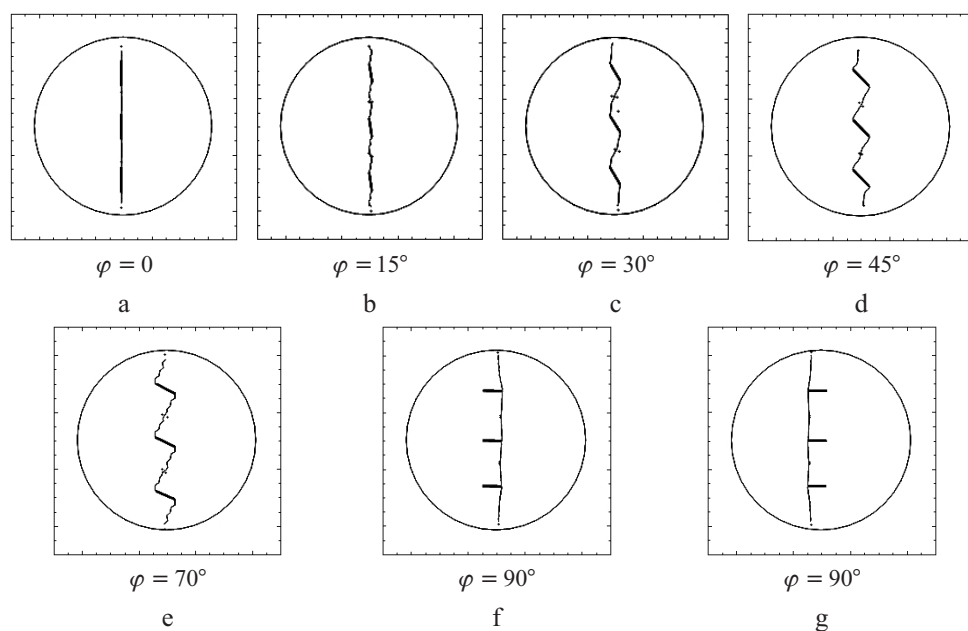

Fig. 7. Numerical simulation of crack coalescence path for disk specimens containing three parallel cracks with equal crack lengths $2b = 10$ mm.

Table 2 compares the numerical and experimental results considering the crack initiation and coalescence stresses. The wing crack initiation stresses for various specimens vary from 1.12–2.32 MPa for the numerical approach and from 0.92–1.86 MPa for the experimental one. The crack coalescence stress varies from 2.25–2.76 MPa for the numerical analysis and from 2.16–2.61 MPa for the experimental one.

4. **Discussion**. The crack propagation process in rock specimens has been studied by several researchers using the CSCBD problem as shown in Fig. 8 [32].

Recently Ghazvinianet al. [33] have experimentally and numerically investigated the crack propagation paths for different crack inclination angles, $\beta = 0, 15, 30, 45,$ and

T a b l e 2

Comparison of Wing Crack Initiation and Crack Coalescence Stresses
(Using the Proposed Numerical Method and the Experimental Data)

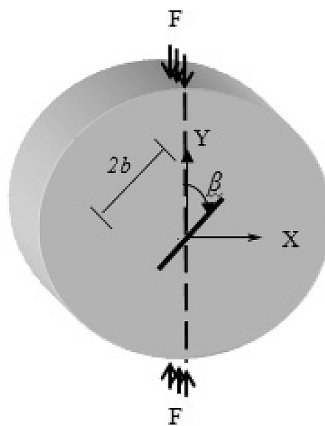| Crack geometry		Wing crack initiation stress (MPa)		Cracks coalescence stress (MPa)	
		Numerical	Experiment	Numerical	Experiment
$\varphi = 0$	Crack 1	2.13	1.74		
	Crack 2	2.24	–	2.7	2.52
	Crack 3	2	1.68		
$\varphi = 15°$	Crack 1	1.91	1.54		
	Crack 2	2	–	2.43	2.28
	Crack 3	1.83	1.68		
$\varphi = 30°$	Crack 1	1.95	1.77		
	Crack 2	1.97	–	2.52	2.31
	Crack 3	1.93	1.67		
$\varphi = 45°$	Crack 1	1.13	0.92		
	Crack 2	1.25	–	2.53	2.44
	Crack 3	1.12	0.95		
$\varphi = 70°$	Crack 1	1.47	1.14		
	Crack 2	1.54	–	2.62	2.42
	Crack 3	1.43	1.28		
$\varphi = 90°$	Crack 1	2.29	1.86		
	Crack 2	2.32	–	2.76	2.61
	Crack 3	2.28	1.79		

Fig. 8. Schematic view of rock-like CSCBD specimen.

60° for CSCBD rock-like specimens. They have used PFC^{2D} code (a discrete element approach based on the finite difference method) to conduct a number of numerical simulations to reproduce their experimental works on CSCBD specimens. Table 3 shows the mechanical properties of rock-like specimens.

Figures 9 and 10 illustrate the experimental data of Ghazvinian et al. [33] and PFC2D simulations of the crack propagation paths in (CSCBD) specimens with different crack inclination angles $\beta = 0, 15, 30, 45,$ and 60°, respectively.

T a b l e 3

Mechanical Properties of Rock-Like Specimens [33]

Characteristic	Parameter	Value
Crack length	$2b$, mm	30
Compressive strength	σ_c, MPa	6.6
Tensile strength	σ_t, MPa	1
Density	γ, kg/m^3	1200

$\beta = 0$ $\beta = 15°$ $\beta = 30°$

$\beta = 45°$ $\beta = 60°$
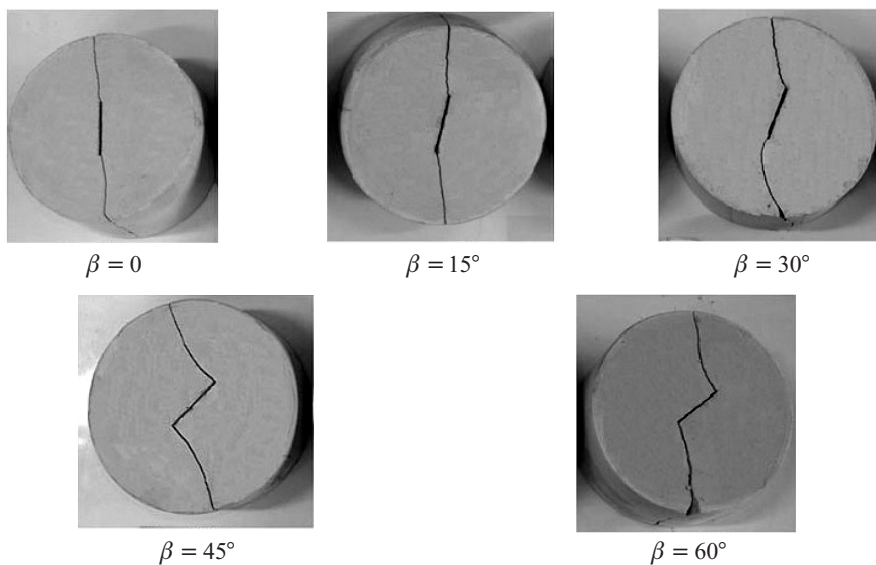
Fig. 9. The crack propagation path in CSCBD specimens with different crack inclination angles $\beta = 0$, 15, 30, 45, and 60° [33].

$\beta = 0$ $\beta = 15°$ $\beta = 30°$

$\beta = 45°$ $\beta = 60°$
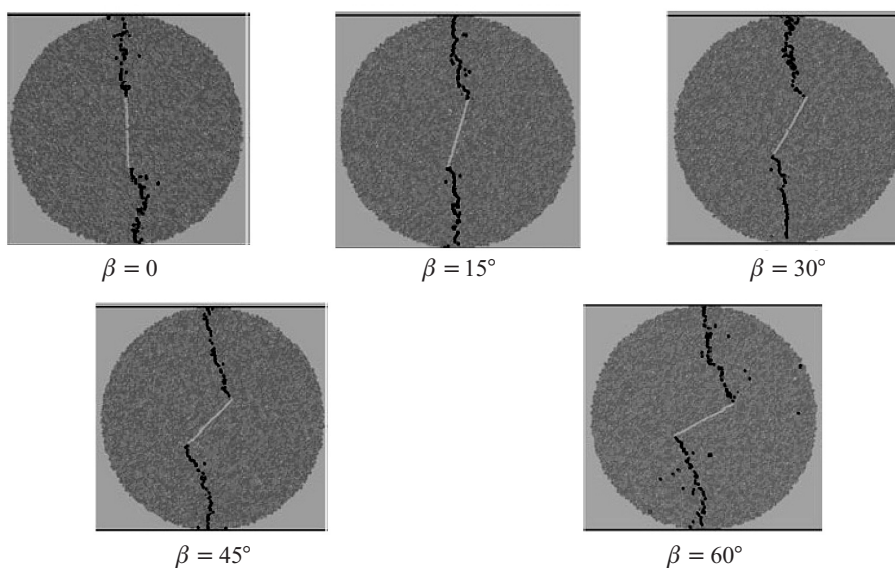
Fig. 10. PFC^{2D} simulation of the propagating paths in (CSCBD) specimens with different crack inclination angles $\beta = 0$, 15, 30, 45, and 60° [33].
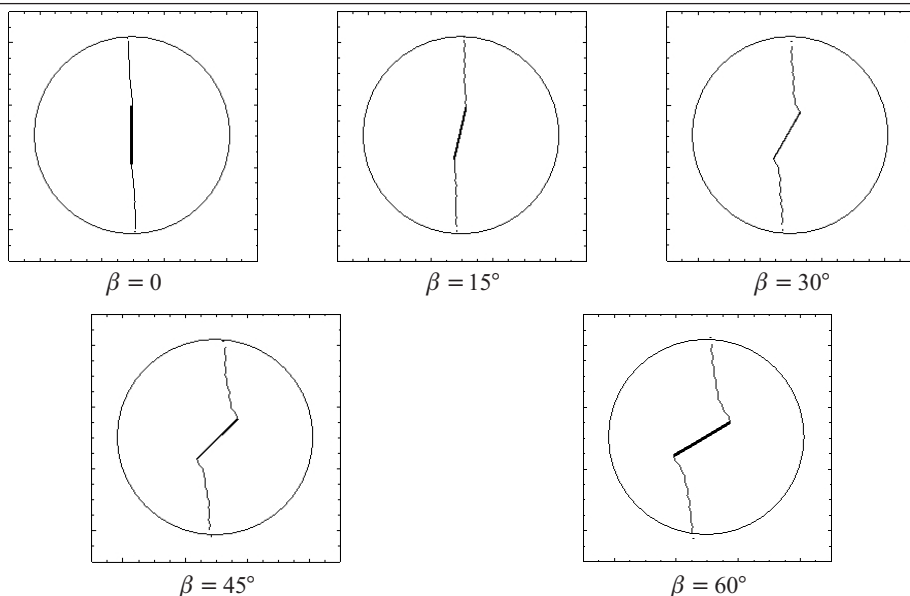
Fig. 11. Boundary element simulation of the crack propagation process in CSCBD specimens.

The crack propagation process in rock-like CSCBD specimens has also been numerically studied by using the higher-order boundary element method proposed in this study. The numerical results obtained by the boundary element simulation of CSCBD specimens are shown in Fig. 11. The numerically simulated crack propagation paths shown in Fig. 11 are in good agreement with the experimental results given by Ghazvinian et al [33] in Fig. 9. Comparative analysis of the results plotted in Figs. 10 and 11 and the experimental data in Fig. 9 clearly demonstrates the accuracy, validity and superiority of the boundary element method results, as compared to those obtained by PFC^{2D} code (Fig. 10). The boundary element code is much faster and user-friendly, because the boundary element method essentially reduces one dimension of the problem and alternatively reduces the mesh size sharply and makes the discretization of the problem simpler and quicker [33].

Conclusions. The crack propagation mechanism of brittle substances has been studied by comprehensive experimental and numerical works in the recent years. This is a complicated process, which requires further efforts to investigate the crack propagation, crack coalescenc in the bridge area, and final fracture paths of the rocks and rock-like materials under compressive line loading. In this study, a detailed analysis of the fracturing process of the precracked rock-like disk specimens was accomplished both by experimental tests and numerical simulation. Effects of fracturing on the breaking load of the precracked rock-like materials are discussed. It is shown that the crack propagation mechanism in the brittle substances due to the crack coalescence phenomenon in the bridge area occurs mainly by propagation of wing cracks emanating from the pre-existing crack tips. The secondary cracks may also be produced after propagation of the wing cracks in the specimens under compressive line loading, but it is experimentally shown that the wing cracks are mainly responsible for the crack coalescence and the final cracks propagating paths. The tested specimens are also numerically simulated by the indirect boundary element method, and the corresponding numerical results show a good fit with the experimental results. The experimental and numerical models properly illustrate initiation of the wing cracks, as well as crack propagation paths produced by the coalescence phenomenon of the three parallel pre-existing cracks in the bridge area.

Р е з ю м е

Проведено випробування на одновісний стиск зразків типу "бразильського диска" зі скальної породи, що мають три попередньо вирощені паралельні тріщини в середній частині. Зразки з модельного матеріалу (бетон на основі пуцоланового портланд-цементу, дрібного піску та води) виготовляли в лабораторії механіки гірських порід. Вимірювання критичного навантаження в таких дисках паказало, що воно несуттєво залежить від орієнтації тріщин і їх взаємовпливу. Процес руйнування зразків вивчали за різних кутів нахилу трьох паралельних тріщин відносно осі стискаючого навантаження за звичайною схемою випробувань бразильських дисків. Експериментально установлено, що на першому етапі навантаження починається біфуркація тріщин та їх розповсюдження в напрямку лінії стискаючого навантаження. Проведено числове моделювання процесу руйнування зразків за допомогою непрямого методу граничних елементів вищого порядку, що відомий як "метод розриву переміщень". Дані числових розрахунків по ініціюванню і злиттю тріщин порівнювали з експериментальними. Отримано тісну кореляцію числових результатів з експериментальними.

1. T. Kato and T. Nishioka, "Analysis of micro–macro material properties and mechanical effects of damaged material containing periodically distributed elliptical microcracks," *Int. J. Fract.*, **131**, 247–266 (2005).

2. Y. Ichikawa, K. Kawamura, K. Uesugi, et al., "Micro- and macrobehavior of granitic rock: observations and viscoelastic homogenization analysis," *Comput. Meth. Appl. Mech. Eng.*, **191**, 47–72 (2001).

3. Z. T. Bieniawski, "Mechanism of brittle fracture of rock. Pt. II. Experimental studies," *Int. J. Rock Mech. Min. Sci. Geomech. Abstr.*, **4**, 407–423 (1967).

4. C. C. Ke, C. S. Chen, and C. H. Tu, "Determination of fracture toughness of anisotropic rocks by boundary element method," *Rock Mech. Rock Eng.*, **41**, 509–538 (2008).

5. E. Hoek and Z. T. Bieniawski, "Brittle rock fracture propagation in rock under compression," *Int. J. Fract. Mech.*, **1**, 137–155 (1965).

6. A. R. Ingraffea, "Fracture propagation in rock," in: Z. P. Bazant (Ed.), *Mechanics of Geomaterials, Rocks, Concrete, Soils*, Wiley, Chichester (1985), pp. 219–258.

7. H. Horii and S. Nemat-Nasser, "Compression-induced microcrack growth in brittle solids: axial splitting and shear failure," *J. Geophys. Res.*, **90**, 3105–3125 (1985).

8. J. F. Huang, G. L. Chen, Y. H. Zhao, and R. Wang, "An experimental study of the strain field development prior to failure of a marble plate under compression," *Tectonophysics*, **175**, 269–284 (1990).

9. B. Shen, O. Stephansson, H. H. Einstein, and B. Ghahreman, "Coalescence of fractures under shear stress experiments," *J. Geophys. Res.*, **100**, 5975–5990 (1995).

10. R. H. C. Wong and K. T. Chau, "Crack coalescence in a rock-like material containing two cracks," *Int. J. Rock Mech. Min. Sci.*, **35**, 147–164 (1998).

11. A. Bobet and H. H. Einstein, "Fracture coalescence in rock-type materials under uniaxial and biaxial compression," *Int. J. Rock Mech. Min. Sci.*, **35**, 863–888 (1998a).

12. R. H. C. Wong, K. T. Chau, C. A. Tang, and P. Lin, "Analysis of crack coalescence in rock-like materials containing three flaws – Part I: experimental approach," *Int. J. Rock Mech. Min. Sci.*, **38**, 909–924 (2001).

13. E. Sahouryeh, A. V. Dyskin, and L. N. Germanovich, "Crack growth under biaxial compression," *Eng. Fract. Mech.*, **69**, 2187–2198 (2002).

14. Y. P. Li, L. Z. Chen, and Y. H. Wang, "Experimental research on pre-cracked marble under compression," *Int. J. Solids Struct.*, **42**, 2505–2516 (2005).

15. C. H. Park and A. Bobet, "The initiation of slip on frictional fractures," in: Proc. of the 41st U.S. Rock Mechanics Symposium, Golden, CO, Paper 06-923 (2006).

16. C. H. Park and A. Bobet, "Crack initiation and propagation from frictional fractures," in: Proc. of the 1st Canada–US Rock Mechanics Symposium (2007), pp. 557–564.

17. C. H. Park, *Coalescence of Frictional Fractures in Rock Materials*, Ph.D. Thesis, Purdue University, West Lafayette, IN (2008).

18. S. Q. Yang, Y. H. Dai, L. J. Han, and Z. Q. Jin, "Experimental study on mechanical behavior of brittle marble specimens containing different flaws under uniaxial compression," *Eng. Fract. Mech.*, **76**, 1833–1845 (2009).

19. C. H. Park and A. Bobet, "Crack coalescence in specimens with open and closed flaws: A comparison," *Int. J. Rock Mech. Min. Sci.*, **46**, 819–829 (2009).

20. C. H. Park and A. Bobet, "Crack initiation, propagation and coalescence from frictional flaws in uniaxial compression," *Eng. Fract. Mech.*, **77**, 2727–2748 (2010).

21. R. P. Janeiro and H. H. Einstein, "Experimental study of the cracking behavior of specimens containing inclusions (under uniaxial compression)," *Int. J. Fract.*, **164**, 83–102 (2010).

22. S. Q. Yang, "Crack coalescence behavior of brittle sandstone specimens containing two coplanar fissures in the process of deformation failure," *Eng. Fract. Mech.*, **78**, 3059–3081 (2011).

23. H. Lee and S. Jeon, "An experimental and numerical study of fracture coalescence in pre-cracked specimens under uniaxial compression," *Int. J. Solids Struct.*, **48**, 979–999 (2011).

24. Cheng-zhi Pu and Ping Cao, "Failure characteristics and its influencing factors of rock-like material with multi-fissures under uniaxial compression," *Trans. Nonferrous Met. Soc. China*, **22**, 185–191 (2012).

25. H. Haeri, K. Shahriar, M. F. Marji, and P. Moarefvand, "On the strength and crack propagation process of the pre-cracked rock-like specimens under uniaxial compression," *Strength Mater.*, **46**, No. 1, 140–152 (2014).

26. M. R. Ayatollahi and M. R. M. Aliha, "On the use of Brazilian disc specimen for calculating mixed mode I–II fracture toughness of rock materials," *Eng. Fract. Mech.*, **75**, 4631–4641 (2008).

27. Q. Z. Wang, "Formula for calculating the critical stress intensity factor in rock fracture toughness tests using cracked chevron notched Brazilian disc (CCNBD) specimens," *Int. J. Rock Mech. Min. Sci.*, **47**, 1006–1011 (2010).

28. F. Dai, R. Chen, M. J. Iqbal, and K. Xia, "Dynamic cracked chevron notched Brazilian disc method for measuring rock fracture parameters," *Int. J. Rock Mech. Min. Sci.*, **47**, 606–613 (2010).

29. F. Dai, K. Xia, H. Zheng, and Y. X. Wang, "Determination of dynamic rock mode-I fracture parameters using cracked chevron notched semi-circular bend specimen," *Eng. Fract. Mech.*, **78**, 2633–2644 (2011).

30. M. R. Ayatollahi and M. Sistaninia, "Mode II fracture study of rocks using Brazilian disk specimens," *Int. J. Rock Mech. Min. Sci.*, **48**, 819–826 (2011).

31. Q. Z. Wang, F. Feng, M. Ni, and X. P. Gou, "Measurement of mode I and mode II rock dynamic fracture toughness with cracked straight through flattened Brazilian disc impacted by split Hopkinson pressure bar," *Eng. Fract. Mech.*, **78**, 2455–2469 (2011).

32. Q. Z. Wang, X. P. Gou, and H. Fan, "The minimum dimensionless stress intensity factor and its upper bound for CCNBD fracture toughness specimen analyzed with straight through crack assumption," *Eng. Fract. Mech.*, **82**, 1–8 (2012).

33. A. Ghazvinian, H. R. Nejati, V. Sarfarazi, and M. R. Hadei, "Mixed mode crack propagation in low brittle rock-like materials," *Arab J. Geosci.*, Accepted Manuscript (2012), DOI 10.1007/s12517-012-0681-8.

34. H. Awaji and S. Sato, "Combined mode fracture toughness measurement by the disk test," *J. Eng. Mater. Technol.*, **100**, 175–182 (1978).

35. J. Sanchez, *Application of the Disk Test to Mode-I–II Fracture Toughness Analysis*, M.S. Thesis, Department of Mechanical Engineering, University of Pittsburgh, Pittsburgh, PA (1979).

36. C. Atkinson, R. E. Smelser, and J. Sanchez, "Combined mode fracture via the cracked Brazilian disk," *Int. J. Fract.*, **18**, 279–291 (1982).

37. D. K. Shetty, A. R. Rosenfield, and W. H. Duckworth, "Mixed mode fracture of ceramic in diametrical compression," *J. Amer. Ceram. Soc.*, **69**, 437–443 (1986).

38. R. J. Fowell and C. Xu, "The use of the cracked Brazilian disk geometry for rock fracture investigations," *Int. J. Rock Mech. Min. Sci. Geomech. Abstr.*, **31**, 571–579 (1994).

39. G. R. Krishnan, X. L. Zhao, M. Zaman, and J. C. Rogiers, "Fracture toughness of a soft sandstone," *Int. J. Rock Mech.*, **35**, 195–218 (1998).

40. K. Khan and N. A. Al-Shayea, "Effects of specimen geometry and testing method on mixed-mode I–II fracture toughness of a limestone rock from Saudi Arabia," *Rock Mech. Rock Eng.*, **33**, 179–206 (2000).

41. N. A. Al-Shayea, K. Khan, and S. N. Abduljauwad, "Effects of confining pressure and temperature on mixed-mode (I–II) fracture toughness of a limestone rock formation," *Int. J. Rock Mech. Rock. Sci.*, **37**, 629–643 (2000).

42. N. A. Al-Shayea, K. Khan, and A. Abdulraheem, "Fracture toughness vs. tensile strength reservoir rocks from Saudi Arabia," in: The 2001 ISRM Sponsored International – 2nd Asian Rock Mechanics Symposium, Beijing, China (2001), pp. 169–172.

43. N. A. Al-Shayea, "Crack propagation trajectories for rocks under mixed mode I–II fracture," *Eng. Geol.*, **81**, 84–97 (2005).

44. F. Erdogan and G. C. Sih, "On the crack extension in plates under loading and transverse shear," *J. Fluids Eng.*, **85**, 519–527 (1963).

45. M. A. Hussian, E. L. Pu, and J. H. Underwood, "Strain energy release rate for a crack under combined mode I and mode II," in: *Fracture Analysis*, ASTM STP 560 (1974), pp. 2–28.

46. G. C. Sih, "Strain-energy-density factor applied to mixed mode crack problems," *Int. J. Fract.*, **10**, 305–321 (1974).

47. B. She and O. Stephansson, "Modification of the G-criterion for crack propagation subjected to compression," *Eng. Fract. Mech.*, **47**, 177–189 (1994).

48. M. F. Marji, H. Hosseinin_Nasab, and A. H. Kohsary, "On the uses of special crack tip elements in numerical rock fracture mechanics," *Int. J. Solids Struct.*, **43**, 1669–1692 (2006).

49. M. F. Marji and I. Dehghani, "Kinked crack analysis by a hybridized boundary element/boundary collocation method," *Int. J. Solids Struct.*, **47**, 922–933 (2010).

50. M. F. Marji, "On the use of power series solution method in the crack analysis of brittle materials by indirect boundary element method," *Eng. Fract. Mech.*, **98**, 365–382 (2013).

51. R. H. C. Wong, C. A. Tang, K. T. Chau, and P. Lin, "Splitting failure in brittle rocks containing pre-existing flaws under uniaxial compression," *Eng. Fract. Mech.*, **69**, 1853–1871 (2002).

52. A. Manouchehrian, M. Sharifzadeh, M. F. Marji, and J. Gholamnejad, "A bonded particle model for analysis of the flaw orientation effect on crack propagation mechanism in brittle materials under compression," *Arch. Civil Mech. Eng.* (2013), (in press).

53. S. L. Crouch, *Analysis of Stresses and Displacements around Underground Excavations: An Application of the Displacement Discontinuity Method*, Geomechanics Report, University of Minnesota, Minneapolis, MN (1967a).

54. H. Guo, N. I. Aziz, and R. A. Schmidt, "Linear elastic crack tip modeling by displacement discontinuity method," *Eng. Fract. Mech.*, **36**, 933–943 (1990).

55. C. Scavia, "Fracture mechanics approach to stability analysis of crack slopes," *Eng. Fract. Mech.*, **35**, 889–910 (1990).

56. M. H. Aliabadi and D. P. Rooke, *Numerical Fracture Mechanics*, Computational Mechanics Publications, Southampton, UK (1991).

57. H. Haeri, K. Shahriar, M. F. Marji, and P. Moarefvand, "Modeling the propagation mechanism of two random microcracks in rock specimens under uniform tensile loading," in: Proc. of 13th Int. Conf. on Fracture, China (2013).

58. H. Haeri, K. Shahriar, M. F. Marji, and P. Moarefvand, "Simulating the bluntness of TBM disc cutters in rocks using displacement discontinuity method," in: Proc. of 13th Int. Conf. on Fracture, China (2013).

59. G. R. Irwin, "Analysis of Stress and strains near the end of a crack," *J. Appl. Mech.*, **24**, 361–364 (1957).

60. M. F. Marji, *Modeling of Cracks in Rock Fragmentation with a Higher Order Displacement Discontinuity Method*, Ph.D. Thesis, Middle East Technical University, Ankara, Turkey (1997).